RCS reduction of integrated antenna arrays with resistive sheets

Gustafsson, Mats

2005

CODEN:LUTEDX/(TEAT-7135)/1-12/(2005)

RCS reduction of integrated antenna arrays with resistive sheets

Mats Gustafsson

Department of Electroscience
Electromagnetic Theory
Lund Institute of Technology
Sweden

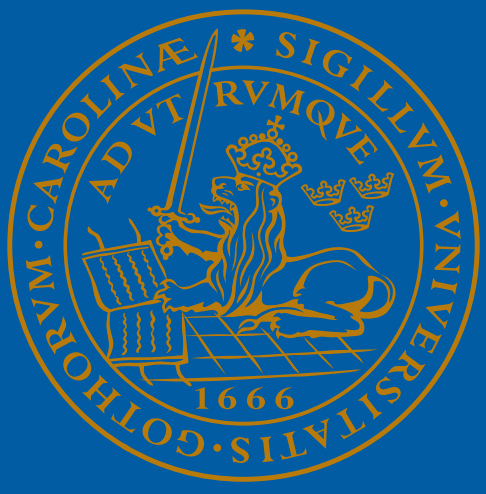

Mats Gustafsson

Department of Electroscience
Electromagnetic Theory
Lund Institute of Technology
P.O. Box 118
SE-221 00 Lund
Sweden

Editor: Gerhard Kristensson

Abstract

Edge diffraction can be a major source of high radar visibility for integrated array antennas. In this paper, it is shown that tapered resistive sheets at the edges of the array can be used to transform the scattering properties of the antenna to that of a metallic plate and hence reduce the radar cross section. Numerical examples of an array of self-complementary patches and a bandpass frequency selective radome are presented to illustrate the results. The RCS reduction is very good for TE polarization but not as efficient for the TM polarization.

1 Introduction

Antennas are a major potential source of high radar visibility on stealth objects. There are several phenomena, *e.g.*, grating lobes, edge diffraction, and surface waves, that contribute to the radar cross section (RCS) of an array antenna. The grating lobes can occur if the inter-element spacing is larger then half a wave length [2, 9, 11]. Edge diffraction can be interpreted as a diffraction by the rapid change in the scattering properties between the antenna and its surrounding [7]. As an antenna is designed to absorb energy in its operational band, the in-band diffraction is significant if the antenna is integrated in a non-absorbing environment. The out of band diffraction can also contribute to the RCS if there is a phase difference between the reflection from the antenna and the reflection from the surrounding.

The specular reflection is in general not a major problem for an integrated antenna as it is directed in the same direction as the specular reflection of the body of the object, *i.e.*, in a safe direction on a stealth object. Although the alignment can reduce the degrading effects of the diffracted waves it is important to reduce their amplitude as it is difficult to avoid backscattered waves as well as multiple scattered waves in the mono-static direction.

Tapered resistive edge treatment can be used to reduce edge diffraction and diffraction from impedance discontinuities [6, 7]. The resistive sheet is highly conductive $\sigma \approx \infty$ and very thin $d \approx 0$, and is such that $\sigma d = R^{-1}$, see *e.g.*, [7, 10, 12]. They are commonly used in radar absorbing materials (RAM) such as Salisbury screens and Jaumann absorbers [7]. They have also been used to taper the edges of antennas to free space [2, 14]. Their scattering properties are analyzed in [4, 13].

In this paper, it is shown that a resistive sheet can transform the scattering properties of the antenna to the scattering properties of a perfectly electric conductor (PEC) in a controlled way. The resistive sheet transforms the reflection coefficient of the infinite antenna along the inverted reactive circles in the Smith chart towards the -1 point as the resistivity decreases to 0. It is shown that the mono-static RCS reduces over a large frequency band and wide scattering angles as long as the physical optics (PO) approximation is accurate. FDTD simulations of the RCS from a self-complementary patch array and an FSS radome are also presented to illustrate the results. The numerical examples indicate a 20 dB reduction of the monostatic RCS in the TE polarization but not as good for the TM case.

2 RCS and physical optics approximation

The RCS, σ, of an object is its equivalent area which if scattered isotropically would result in the same scattered power density [8]. It can be determined as the quotient between the scattered wave and the incident wave, *i.e.*,

$$\sigma(\hat{\boldsymbol{r}},\hat{\boldsymbol{k}}) = \lim_{r\to\infty} 4\pi r^2 \frac{|\boldsymbol{E}_{\mathrm{s}}(r,\hat{\boldsymbol{r}})|^2}{|\boldsymbol{E}_{\mathrm{i}}(\hat{\boldsymbol{k}})|^2} = \frac{4\pi}{k^2}\frac{|\boldsymbol{F}_{\mathrm{s}}(\hat{\boldsymbol{r}})|^2}{|\boldsymbol{E}_{\mathrm{i}}(\hat{\boldsymbol{k}})|^2}, \tag{2.1}$$

where the incident wave $\boldsymbol{E}_{\mathrm{i}}$ is a plane wave $\boldsymbol{E}_{\mathrm{i}}(\boldsymbol{x};\hat{\boldsymbol{k}}) = \boldsymbol{E}_0 \mathrm{e}^{-\mathrm{i}k\hat{\boldsymbol{k}}\cdot\boldsymbol{x}}$. The RCS depends on the polarization and frequency of the incident wave. For two-dimensional objects the RCS is the equivalent length of the object.

Here, we analyze the contribution to the RCS from an antenna integrated in a surface of a PEC object. We assume that the antenna array is planar and that it is integrated in an infinite planar PEC surface in the xy-plane, see Figure 1. The scattered field can be determined from the currents on the surface of the object. It is natural to consider the difference between the scattered field from the object with the antenna and the scattered field from the object when the antenna is replaced with PEC.

The totally scattered field can be represented with a Fourier type integral of the equivalent electric surface current, $\boldsymbol{J}$, and magnetic surface current, $\boldsymbol{M}$, over the xy-plane [11]. We get an infinite planar PEC surface when the antenna is replaced with PEC. The surface current on the infinite planar PEC surface is given by $\boldsymbol{J}_0 = 2\hat{\boldsymbol{z}} \times \boldsymbol{H}_{\mathrm{i}}$ or equivalently by a reflection coefficient $\rho_0 = -1$. Subtraction with $\boldsymbol{J}_0$ over the hole surface gives the antenna contribution to the scattered field. The antenna contribution to the scattered far-field is, hence, given as a Fourier integral over the xy-plane, *i.e.*,

$$\boldsymbol{F}_{\mathrm{s}}(\hat{\boldsymbol{r}}) = \frac{\mathrm{i}k^2}{4\pi}\hat{\boldsymbol{r}} \times \iint_{\mathbb{R}^2} \big(\boldsymbol{M}(\boldsymbol{x}) - \eta_0 \hat{\boldsymbol{r}} \times \big(\boldsymbol{J}(\boldsymbol{x}) - \boldsymbol{J}_0(\boldsymbol{x})\big)\big)\mathrm{e}^{\mathrm{i}k\hat{\boldsymbol{r}}\cdot\boldsymbol{x}}\,\mathrm{dS}. \tag{2.2}$$

We analyze the RCS in an approximation where the local reflection coefficient is determined in the physical optics approximation (PO). For periodic antenna arrays and FSS, we use the reflection coefficients of the infinite periodic cases. Observe that PO is not very accurate for the diffracted field. The physical theory of diffraction (PTD) could be used to improve the accuracy. However, PO illustrates the basic phenomena and it is sufficient for our analysis in this paper. Unfortunately, the PO approximation of the aperture currents is not unique and not necessarily consistent with the boundary conditions on the infinite ground plane surrounding the aperture [11, Ch. 16]. To obtain a scattered field that is consistent with the boundary condition on the PEC screen, we need to use an approximation using only magnetic currents [11, Ch. 16]. The magnetic currents are given by

$$\boldsymbol{M}(\boldsymbol{x}) = 2\rho(\boldsymbol{x})\hat{\boldsymbol{z}} \times \boldsymbol{E}_{\mathrm{i}}(\boldsymbol{x}) = 2\rho(\boldsymbol{x})\hat{\boldsymbol{z}} \times \boldsymbol{E}_0 \mathrm{e}^{-\mathrm{i}k\hat{\boldsymbol{k}}\cdot\boldsymbol{x}}, \tag{2.3}$$

where $\rho(\boldsymbol{x})$ is the reflection coefficient.

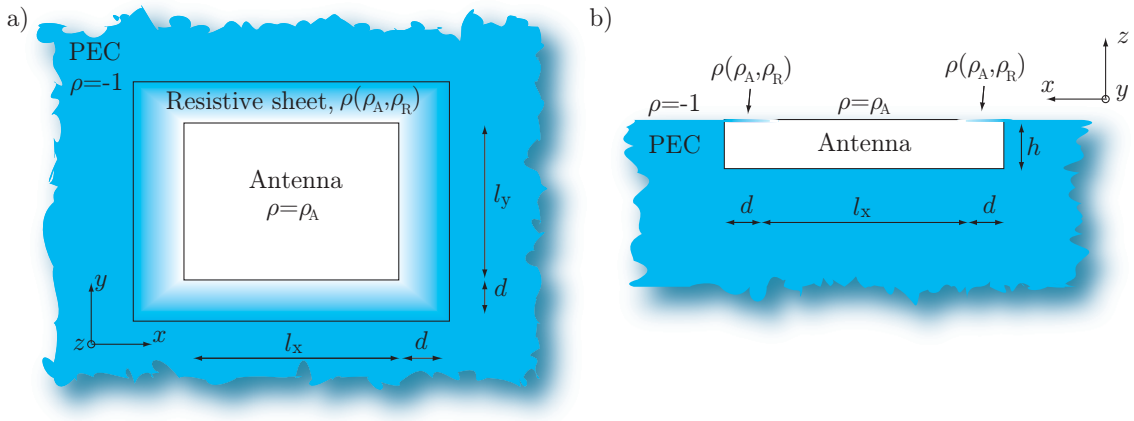

Figure 1: Illustration of the integrated antenna. The resistive sheet at the edges of the antenna transforms the reflection coefficient of the antenna, ρ_{A}, to -1 over the transition zone with width d. a) top view. b) side view.

The reflection coefficient can be dyadic. However, it is sufficient to consider scalar reflection coefficients for the present analysis. The reflection coefficient depends on the spacial coordinate $\boldsymbol{x}$, the frequency f, direction $\hat{\boldsymbol{k}}$, and the polarization $\boldsymbol{E}_{\mathrm{i}}$. We also need to replace the surface current, $\boldsymbol{J}_0$, with an equivalent magnetic surface current, $\boldsymbol{M}_0$. Here, we use that a magnetic surface current $\boldsymbol{M}_0 = -2\hat{\boldsymbol{z}} \times \boldsymbol{E}_{\mathrm{i}}$ gives an identical reflected field as the electrical current $\boldsymbol{J}_0 = 2\hat{\boldsymbol{z}} \times \boldsymbol{H}_{\mathrm{i}}$. Substitution of the magnetic surface PO currents into (2.2) gives the PO approximation of the far-field, *i.e.*,

$$\boldsymbol{F}_{\mathrm{s}}(\hat{\boldsymbol{r}}) = \frac{\mathrm{i}k^2}{2\pi}\hat{\boldsymbol{r}} \times (\hat{\boldsymbol{z}} \times \boldsymbol{E}_0) \iint_A \big(\rho(\boldsymbol{x}) + 1\big)\mathrm{e}^{-\mathrm{i}k(\hat{\boldsymbol{k}}-\hat{\boldsymbol{r}})\cdot\boldsymbol{x}}\,\mathrm{dS} \tag{2.4}$$

where A denotes the aperture. This gives the physical optics approximation of the RCS

$$\sigma(\hat{\boldsymbol{r}}, \hat{\boldsymbol{k}}) = \frac{k^2|\boldsymbol{p}|^2}{\pi}\left|\iint_A \big(\rho(\boldsymbol{x}) + 1\big)\mathrm{e}^{-\mathrm{i}k(\hat{\boldsymbol{k}}-\hat{\boldsymbol{r}})\cdot\boldsymbol{x}}\,\mathrm{dS}\right|^2 \tag{2.5}$$

where $\boldsymbol{p} = \hat{\boldsymbol{r}} \times (\hat{\boldsymbol{z}} \times \boldsymbol{E}_0)/|\boldsymbol{E}_0|$. For TE and TM polarization, we have $|\boldsymbol{p}|^2 = \cos^2\theta_{\mathrm{r}}$ and $|\boldsymbol{p}|^2 = \cos^2\theta_{\mathrm{i}}$, where θ_{r} and θ_{i} denote the scattering and incident angles, respectively. Here, it is seen that the result is consistent with the boundary conditions, *i.e.*, the reflection coefficient approaches zero for grazing angles in the TE case. However, it is also well known that the accuracy of the PO approximation decreases for large scattering angles. This is also seen in the comparison with FDTD simulations in Section 4.2. In this paper, we focus on the monostatic RCS, *i.e.*, $\hat{\boldsymbol{r}} = -\hat{\boldsymbol{k}}$, of planar objects in the xy-plane with a scan angle θ where in both cases TE and TM we have $|\boldsymbol{p}| = \cos\theta$.

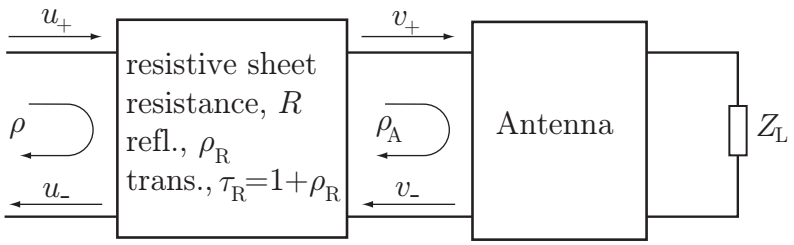

Figure 2: Illustration of the scattering model with a resistive sheet in front of the antenna. The resistive sheet with resistivity R and the antenna with load $Z_{\rm L}$ has the reflection coefficients $\rho_{\rm R}$ and $\rho_{\rm A}$, respectively.

3 Resistive sheet

To reduce the diffracted field we need to construct a smooth transition over the interface. Here, we consider a resistive sheet with high conductivity, *i.e.*, thickness $d \to 0$ and conductivity $\sigma \to \infty$, with d and σ such that $\sigma d = R^{-1}$ is finite. The reflection coefficient of the sheet is [10]

$$\rho_{\rm R} = \frac{-\eta_{\rm T}}{2R + \eta_{\rm T}}, \tag{3.1}$$

where $\eta_{\rm T}$ is the transverse wave impedance [11], *i.e.*, $\eta_{\rm TE} = \eta_0/\cos\theta$ and $\eta_{\rm TM} = \eta_0 \cos\theta$ where θ is the incident angle. It is easily seen that $\rho_{\rm R}$ is real valued and $-1 \le \rho_{\rm R} \le 0$. The corresponding transmission coefficient is given by $\tau_{\rm R} = 1 + \rho_{\rm R}$.

We use a resistive sheet placed at the edges in front of the antenna array as seen in Figure 1. Let the resistance be zero (PEC) at the edge of the antenna and increase to infinity (air) at distance d from the edge. The reflection coefficient of the combined resistive sheet and antenna structure is analyzed in the PO approximation with the circuit model shown in Figure 2. The scattering properties of the antenna array is modeled with the reflection coefficient $\rho_{\rm A}$. The reflection coefficient is small in the frequency band where the antenna is matched to the load $Z_{\rm L}$. However, as $\rho_{\rm A}$ depends on the frequency, the incident angle, and the polarization, it is difficult to utilize the specific structure of $\rho_{\rm A}$ in the analysis. Here, we consider $\rho_{\rm A}$ as an arbitrary complex valued number in the unit circle, *i.e.*, $|\rho_{\rm A}| \le 1$. The reflection coefficient of the combined sheet and antenna is obtained with a standard scattering analysis [11, Ch. 12]. The scattered waves depicted in Figure 2 are related as $u_- = \rho u_+$, $v_- = \rho_{\rm A} v_+$, $v_+ = \rho_{\rm R} v_- + \tau_{\rm R} u_+$, and $u_- = \rho_{\rm R} u_+ + \tau_{\rm R} v_-$. Elimination of the $v_\pm$ waves gives the total reflection coefficient

$$\rho(\rho_{\rm A}, \rho_{\rm R}) = \rho_{\rm R} + \frac{\rho_{\rm A}\tau_{\rm A}^2}{1 - \rho_{\rm R}\rho_{\rm A}} = \frac{\rho_{\rm R} + \rho_{\rm A} + 2\rho_{\rm R}\rho_{\rm A}}{1 - \rho_{\rm R}\rho_{\rm A}}. \tag{3.2}$$

We consider the map from $\rho_{\rm A}$ to ρ for fixed parameters $\rho_{\rm R}$. This is a conformal map, mapping circles in the complex valued $\rho_{\rm A}$-plane into circles in the complex valued ρ-plane [1]. It is easily seen that $\rho(-1, \rho_{\rm R}) = -1$, *i.e.*, PEC is transformed to PEC.

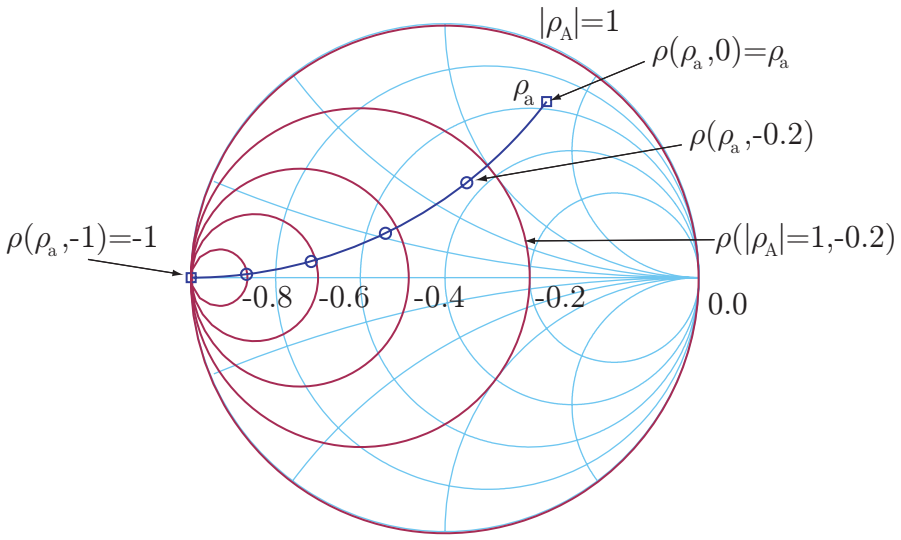

Figure 3: Transformation of the reflection coefficient $\rho_{\rm A} \mapsto \rho(\rho_{\rm A}, \rho_{\rm R})$. An arbitrary reflection coefficient $\rho_{\rm a}$ is transformed along the 'inverted' reactive circles to the point -1 as $\rho_{\rm R} : 0 \to -1$. The unit circle $|\rho_{\rm A}| = 1$ is mapped into circles $\rho(|\rho_{\rm A}| = 1, \rho_{\rm R})$ as illustrated for $\rho_{\rm R} = -0.2, -0.4, -0.6, -0.8$.

The transformation properties of the unit circle, $|\rho_{\rm A}| = 1$, are constructed with the additional relation $\rho(1, \rho_{\rm R}) = (1 + 3\rho_{\rm R})/(1 - \rho_{\rm R})$. This gives that the unit circle, $|\rho_{\rm A}| = 1$, is mapped into the circle centered at

$$\frac{2\rho_{\rm R}}{1-\rho_{\rm R}} = \frac{-\eta_{\rm T}}{R+\eta_{\rm T}} \quad \text{with radius} \quad \frac{1+\rho_{\rm R}}{1-\rho_{\rm R}} = \frac{R}{R+\eta_{\rm T}}. \tag{3.3}$$

The circles corresponding to $\rho_{\rm R} = -0.2, -0.4, -0.6, -0.8$ are shown in Figure 3. An arbitrary antenna reflection coefficient $\rho_{\rm a}$ is hence transformed towards the point -1, *i.e.*, PEC, as $\rho_{\rm R} : 0 \to -1$ or equivalently $R : \infty \to 0$. As the reflection coefficient of the resistive sheet, $\rho_{\rm R}$ follows a line, *i.e.*, a generalized circle [1], the total reflection coefficient, ρ, follows a circle towards -1. These circles are given by the 'inverted' reactive circles, see Figure 3. The effect of the resistive sheet can also be interpreted as a parallel coupling between the sheet resistivity R and the antenna impedance seen from the outside, $Z_{\rm A} = \eta_{\rm T}(1 + \rho_{\rm A})/(1 - \rho_{\rm A})$.

The RCS (2.5) is easily evaluated for an arbitrary transition zone. To illustrate the effectiveness of the conducting sheet, we consider an example with a piecewise constant, a linear, and cubic spline interpolation of the reflection coefficient, see Figure 4a. The corresponding one-dimensional Fourier transforms are shown in Figure 4b. Here, it is seen that the resistive tapering reduces the RCS. There is no major difference between the three cases for low frequencies, *i.e.*, $\lambda > \lambda_0 \approx$ length of transition zone. For higher frequencies, the improvement is larger for the smooth transition, see also [7, Ch. 8].

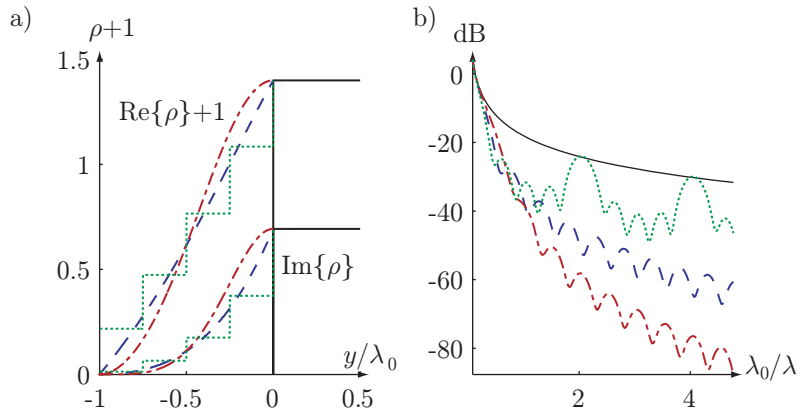

Figure 4: a) transition of the reflection coefficient from $\rho_A + 1$ to 0 with a piecewise constant, a linear, and a cubic spline interpolation. b) the corresponding Fourier transforms in dB.

4 Numerical examples

Numerical simulations are used to illustrate the reduction of the RCS for an antenna array and an FSS bandpass radome. To emphasize the edge diffracted part, we consider infinite times finite arrays, *i.e.*, periodic boundary conditions are used in one dimension. Here, the code periodic boundary FDTD (PB-FDTD) developed by H. Holter [5] is used for the numerical simulations.

4.1 Self-complementary patch array

As a first example, we consider an infinite antenna array consisting of PEC patches and dielectric sheets as depicted in Figure 5ac. The patches are fed at the corners of each patch. Here, we focus on a receiving array where the feeds are terminated in a characteristic impedance $Z_0 = 120\,\Omega$. The patch array is almost self complementary, *i.e.*, the PEC structure is almost identical to its complement. Hence, the impedance of the patch array is frequency independent if situated in free space [3, 8]. As the patch array radiates bidirectional, the ground plane under the patches defines the resonance frequency, f_0, from $h = \lambda_0/4 = c_0/(4f_0)$. The dielectric sheets above the patch array act as a filter matching the antenna for a large range of frequencies. In analogy with quarter-wave transformers in broadband matching, the sheets are chosen to be of equal optical thickness, *i.e.*, a sheet thickness of $d_i = h\epsilon_i^{-1/2}$ is used [3, 9, 11]. A typical reflection coefficient normalized to $Z_0 = 120\,\Omega$ is shown in Figure 5b.

Here, we consider a patch array with dimensions $a = 9.6\,\text{mm}$, $b = 0.8\,\text{mm}$, and $h = 13.6\,\text{mm}$ giving the unit-cell length $l_0 = 20.8\,\text{mm}$. This gives a resonance frequency around 5.5 GHz and the onset of grating lobes at 7.5 GHz. Dielectric sheets with permittivities $\epsilon_1 = 7$ and $\epsilon_2 = 3$ are used. We consider an array consisting of 20 unit cells in the y-direction, giving $l = 20l_0 = 416\,\text{mm}$, and an infinite amount of unit cells in the x-direction, *i.e.*, periodic boundary conditions in the x-direction. As

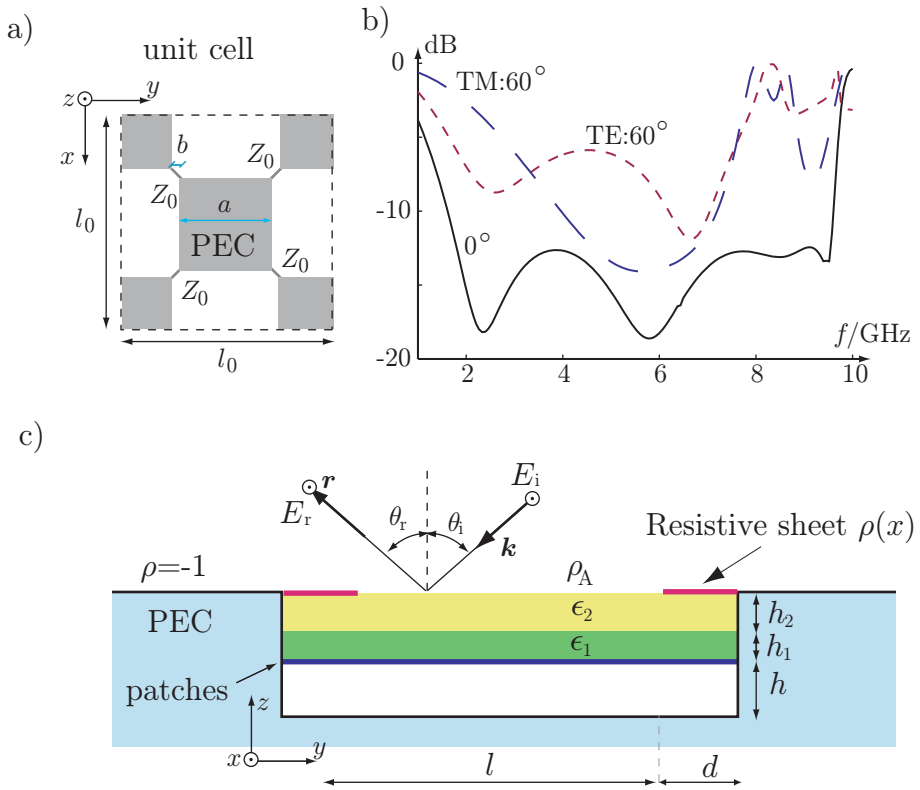

Figure 5: Illustration of the integrated antenna array. a) top view of the element geometry. The infinite array consists of a periodic repetition of square perfectly electric conductor (PEC) patches fed at the corners. An impedance $Z_0 = 120\,\Omega$ is used to model the feed for the receiving antenna. b) calculated reflection coefficient for the infinite patch antenna as a function of the frequency for $\theta = 0°, 60°$. c) scattering model of the patch array with resistive sheets at the edges. We use 20 unit cells in the aperture, *i.e.*, $l = 20l_0$.

a plane wave in the yz-plane impinges on the array, it is convenient to use the polar angles θ in the range $-\pi/2 \leq \theta \leq \pi/2$. The bistatic RCS of the patch array for the incident angle 60° and TE polarization is depicted in Figure 6a. As expected, the specular reflection at $-60°$ dominates the bistatic RCS. The oscillations of the RCS away from the specular direction are due to the constructive and destructive interference of the edge diffracted waves. The oscillations are more rapid for large arrays. The envelope of the RCS is highlighted to emphasize the amplitude of the diffracted waves and at the same time deemphasize the dependence of the size of the array. The monostatic RCS is approximately $-20\,$dBm at 3 GHz and $-25\,$dBm at 5 GHz for the integrated array without tapering. With a linear tapering over two unit cells, *i.e.*, $d = 2l_0 \approx 42\,$mm, the monostatic RCS reduces with approximately 20 dBm.

The resistive tapering reduces the RCS by smoothing out the discontinuity between the antenna and its surrounding material. However, the RCS of an array can

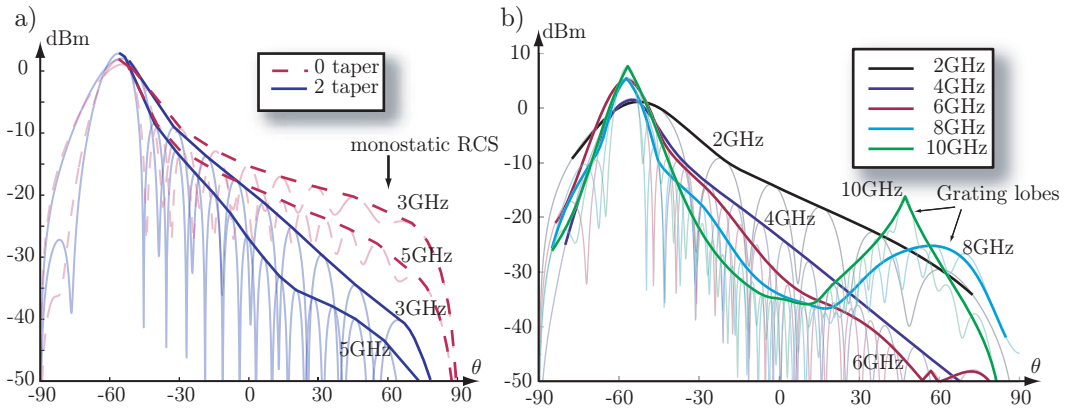

Figure 6: Calculated (FDTD) bi-static RCS of a self-complementary patch array illuminated from $\theta = 60°$ in TE polarization. The envelope of the RCS is included to emphasized contribution from edge diffraction. a) with and without resistive sheets at 3 GHz and 5 GHz. b) linearly tapered with a resistive sheet over two unit cells for $2, 4, 6, 8, 10$ GHz.

be significant if the array supports gating lobes. These grating lobes can occur if the inter-element spacing in the array is larger than half a wavelength. The patch array supports grating lobes for frequencies above 7.5 GHz. The RCS of the self-complementary $24 \times \infty$ patch array with a linear resistive tapering over the 2 edge elements for an illumination from $\theta = 60°$ at $2, 4, 6, 8, 10$ GHz is shown in Figure 6b. As seen in the figure, the monostatic RCS is very small for frequencies up to the onset of grating lobes at 7.5 GHz. The beam width of the grating lobes as well as the specular lobe depends on the size of the array. The beam width decreases for larger arrays.

4.2 FSS bandpass radome

We also consider the RCS of an FSS integrated radome. We consider a symmetric hybrid radome with four-legged loop elements [8], see Figure 7a. The elements are arranged in a square grid with side length of $l_0 = 6.6$ mm and they have a slot width of 0.17 mm. The loop elements are placed in a 3 mm thick dielectric sheet with permittivity $\epsilon_r = 1.6$. This gives a bandpass structure with passband from 8.5 GHz to 9 GHz as seen in Figure 8a.

The radome is integrated into a PEC structure and an antenna is placed under the radome, see Figure 7b. Here, we use the patch array described in Section 4.1 tuned to 8.5 GHz. The upper dielectric sheet is placed 5 mm from the inner side of the radome. We consider the three cases: without tapering, with a 26 mm linear taper, and with a 53 mm linear taper. The radome size excluding the taper is 332 mm $\times$ ∞. The finite length corresponds to 50 unit cells. The bistatic RCS is shown in Figure 8bcd for a TE wave at 45° and the frequencies $6, 8.5, 11$ GHz. The envelope of the RCS is highlighted to emphasize the amplitude of the edge diffracted part. As

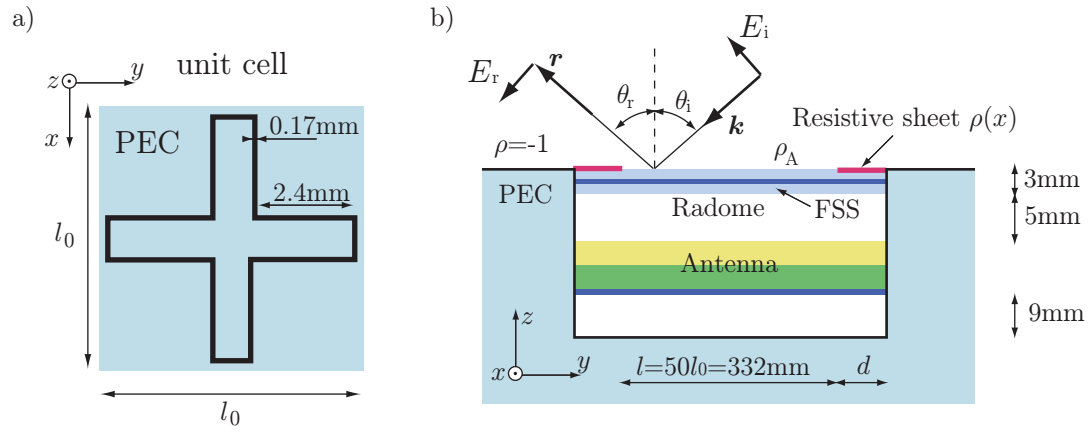

Figure 7: Geometry of the FSS bandpass radome structure. a) unit cell. b) side view with the radome and the antenna.

expected the specular reflection is largest in the passband, *i.e.*, at 8.5 GHz, where the radome discontinuity between the radome and PEC is large. For frequencies outside the passband, the radome is highly reflecting and the discontinuity smaller. The effect of the tapering is negligible in the specular reflection.

The monostatic RCS is also largest in the passband. Here, the effect of the tapering is considerable. As seen in Figure 8c, the tapering reduces the monostatic RCS with 15 dBm to 20 dBm. The monostatic RCS is also reduced outside the passband with the tapering, however the improvement is not as large as the original RCS is much smaller. In Figure 9a, a comparison between the bistatic RCS calculated with FDTD and with the PO approximation is shown. The envelope of the FDTD and PO results are given by the solid and dashed curves, respectively. It is seen that the PO approximation gives a rough estimate of the RCS for the TE case.

The examples above illustrate the effectiveness of the resistive tapering and indicate that the PO analysis is reliable for TE polarization. The resistive sheets are not as effective for the TM case. Figure 9bcd, shows a comparison between FDTD simulations and PO approximation of the bistatic RCS of the FSS radome in TM polarization. Here, it is seen that the PO and the FDTD results are only consistent in the specular direction. The PO approximation underestimates the monostatic RCS and the bistatic RCS for large scattering angles. It is also seen that the resistive tapering is not as efficient as in the TE case. This can be attributed to at least two more or less related effects. First the TM polarization supports surface waves above the PEC ground plane. Secondly, the reflection coefficient of the resistive sheet approaches zero for grazing angles. Hence, a surface wave generated by the edge diffraction can propagate along the structure and is not absorbed by the resistive sheet. To improve the RCS even further it is necessary to reduce the degrading effect of the surface waves. One possible design is to continue the region under the PEC surface and fill it with RAM.

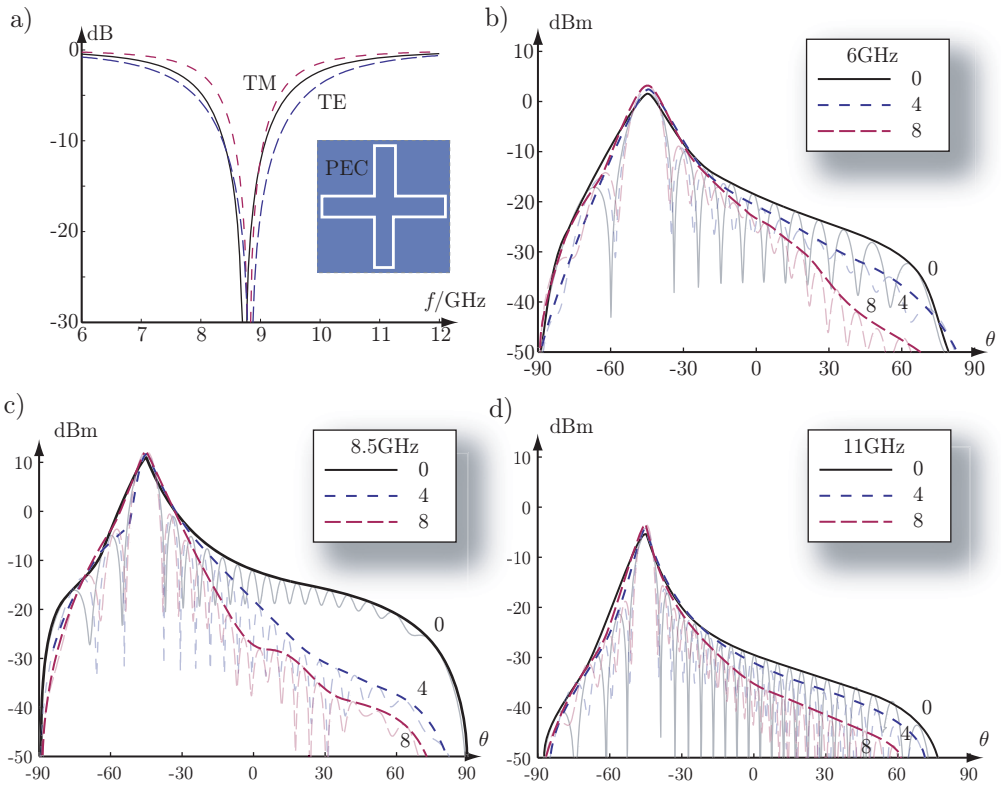

Figure 8: Calculated (FDTD) bistatic RCS of an FSS bandpass radome. a) reflection coefficient of the infinite times infinite radome for 0°, TE 45°, and TM 45°. bcd) a $50 \times \infty$ array illuminated from $\theta = 45°$ in TE polarization for a linear resistive tapering of $0, 26, 53$ mm. The envelope of the RCS is highlighted to emphasize the contributions from the edge diffraction and the grating lobes. b) 6 GHz. c) 8.5 GHz. d) 11 GHz.

5 Conclusions

In this paper it is shown that tapered resistive sheets can reduce the monostatic RCS of antenna arrays and bandpass radomes for TE polarization. The resistive sheet transforms the reflection coefficient of the antenna or radome to that of a PEC. The RCS is reduced by elimination of the edge diffracted field. To obtain a low RCS for higher frequencies it is also necessary to use a structure without grating lobes. The antenna performance is of course affected by the resistive sheet. However as the transition zone is of the order of a wavelength, the effect should not be a major concern for large arrays. The effectiveness for TM polarization is not as clear and more analysis is needed for this case.

Acknowledgment

This work was supported by the NFFP3+ project 521 SIG-SUAV.

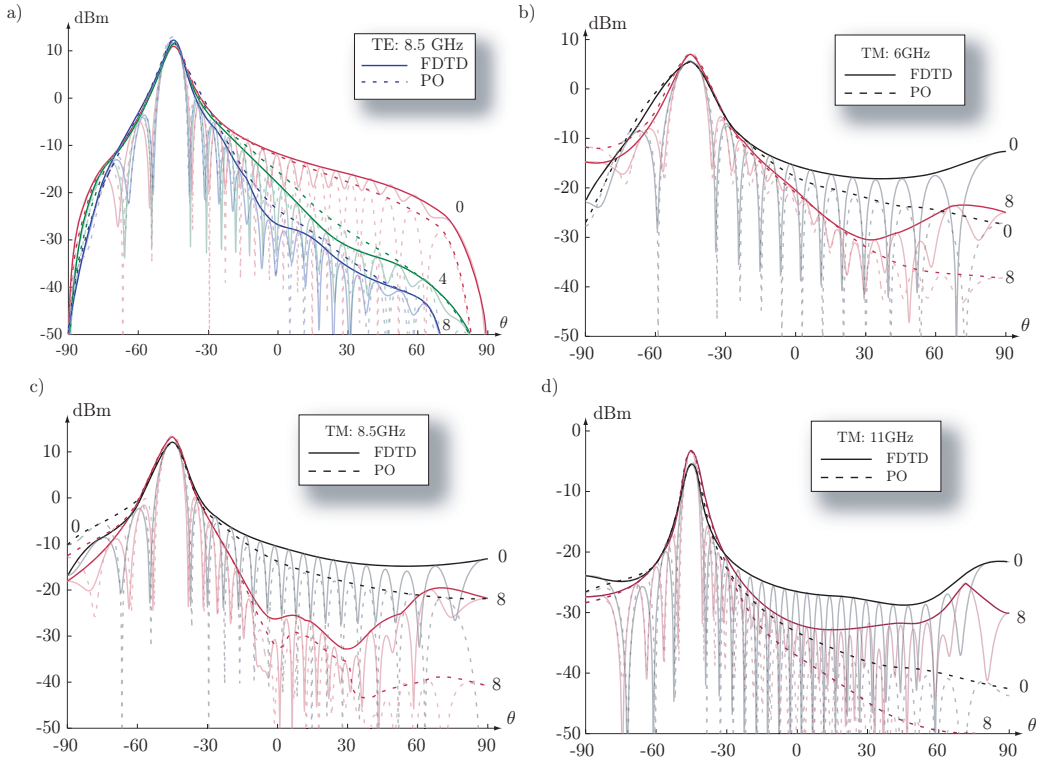

Figure 9: Comparison between the FDTD and PO bistatic RCS of the FSS bandpass radome. a) TE polarization at 45° with edge tapers of $0, 26, 53$ mm. bcd) TE polarization at 45° a 53 mm with edge tapers of $0, 53$ mm.

References

[1] G. B. Arfken and H. J. Weber. *Mathematical Methods for Physicists.* Academic Press, New York, fifth edition, 2001.

[2] J. David Lynch. *Introduction to RF Stealth.* SciTech Publishing Inc., 5601 N. Hawthorne Way, Raleigh, NC 27613, 2004.

[3] M. Gustafsson. Broadband array antennas using a self-complementary antenna array and dielectric slabs. Technical Report LUTEDX/(TEAT-7129)/1–8/(2004), Lund Institute of Technology, Department of Electroscience, P.O. Box 118, S-221 00 Lund, Sweden, 2004. `http://www.es.lth.se`.

[4] R. L. Haupt and V. V. Liepa. Synthesis of tapered resistive strips. *IEEE Trans. Antennas Propagat.*, **35**(11), 1217–1225, 1987.

[5] H. Holter and H. Steyskal. Infinite phased-array analysis using FDTD periodic boundary conditions—pulse scanning in oblique directions. *IEEE Trans. Antennas Propagat.*, **47**(10), 1508–1514, 1999.

[6] E. F. Knott. Suppression of edge scattering with impedance strings. *IEEE Trans. Antennas Propagat.*, **45**(12), 1768–1773, 1997.

[7] E. F. Knott, J. F. Shaeffer, and M. T. Tuley. *Radar Cross Section.* SciTech Publishing Inc., 5601 N. Hawthorne Way, Raleigh, NC 27613, 2004.

[8] J. D. Kraus and R. J. Marhefka. *Antennas.* McGraw-Hill, New York, third edition, 2002.

[9] B. Munk. *Finite Antenna Arrays and FSS.* John Wiley & Sons, New York, 2003.

[10] J. R. Natzke and J. L. Volakis. Characterization of a resistive half plane over a resistive sheet. *IEEE Trans. Antennas Propagat.*, **41**(8), 1063–1068, 1993.

[11] S. J. Orfanidis. Electromagnetic waves and antennas, 2002. `www.ece.rutgers.edu/~orfanidi/ewa`, revision date June 21, 2004.

[12] T. B. A. Senior. Backscattering from resistive strips. *IEEE Trans. Antennas Propagat.*, **27**(6), 808–813, 1979.

[13] T. B. A. Senior and V. V. Liepa. Backscattering from tapered resistive strips. *IEEE Trans. Antennas Propagat.*, **32**(7), 747–751, 1984.

[14] J. L. Volakis, A. Alexanian, and J. M. Lin. Broadband RCS reduction of rectangular patch by using distributed loading. *Electronics Letters*, **28**(25), 2322–2323, 1992.